

# Signatures of inflow motion in cores of massive star formation: Potential collapse candidates

Yuefang Wu<sup>1</sup>, Christian Henkel<sup>2</sup>, Rui Xue<sup>1,3</sup>, Xin Guan<sup>1</sup>, Martin Miller<sup>4</sup>

## ABSTRACT

Using the IRAM 30 m telescope, a mapping survey in optically thick and thin lines was performed towards 46 high mass star-forming regions. The sample includes UC HII precursors and UC HII regions. Seventeen sources are found to show "blue profiles", the expected signature of collapsing cores. The excess of sources with blue over red profiles ( $[N_{\text{blue}} - N_{\text{red}}]/N_{\text{total}}$ ) is 29% in the  $\text{HCO}^+ J=1-0$  line, with a probability of 0.6% that this is caused by random fluctuations. UC HII regions show a higher excess (58%) than UC HII precursors (17%), indicating that material is still accreted after the onset of the UC HII phase. Similar differences in the excess of blue profiles as a function of evolutionary state are not observed in low mass star-forming regions. Thus, if confirmed for high mass star-forming sites, this would point at a fundamental difference between low- and high-mass star formation. Possible explanations are inadequate thermalization, stronger influence of outflows in massive early cores, larger gas reserves around massive stellar objects or different trigger mechanisms between low- and high-mass star formation.

*Subject headings:* ISM: molecules — ISM: kinematic and dynamics — stars: formation — radio lines: ISM

---

<sup>1</sup>Department of Astronomy, Peking Univ., 100871 Beijing, China, yfwu@bac.pku.edu.cn

<sup>2</sup>Max-Planck-Institut für Radioastronomie, Auf dem Hügel 69, 53121 Bonn, Germany

<sup>3</sup>Present affiliation: National Astronomical Observatory, Chinese Academy of Sciences, 100012 Beijing, China

<sup>4</sup>I. Physikalisches Institut der Universität zu Köln, Zùlpicher Straße 77, 50937, Köln, Germany

## 1. Introduction

Inflow motion is a fundamental phenomenon during stellar formation. Although the search for inflow is usually more difficult than that for outflow, studies of inflow have made great progress since the 1990s. In low-mass star forming regions, inflow motions were detected at different evolutionary stages, including Class –I, Class 0 and Class I cores (Zhou et al. 1993; Mardones et al. 1997; Lee, Myers, & Tafalla 1999; Gregersen et al. 2000; Evans 2003). Recently, a number of inflow candidates were found in high mass star formation regions. Among a sample of 28 massive cores, 12 were found to show line profiles that peak at blue-shifted velocities (hereafter ”blue profiles”; see Sect. 3.1), the expected signature of inflow (Wu & Evans 2003). Fuller, Williams, & Sridharan (2005) (hereafter FWS05) detected such asymmetric profiles in 22 cores within a sample of 77 high-mass proto-stellar objects (HMPOs). Most recently, Wyrowski et al. (2006) detected 9 sources with a blue profile in a sample of 12 ultracompact (UC) HII regions.

Variation of inflow motion with time is critical for high mass star formation. It has been indicated that when a protostar reaches  $>10 M_{\odot}$  it can generate enough radiation pressure to halt spherical infall and inhibit its mass increasing (Wolfire & Cassinelli 1987). Observationally, however, it is not yet clear how inflow is related to the evolution of massive (proto)stars. To study this problem, we have carried out a survey for a sample including both cores of UC HII regions and precursors of UC HII regions.

While previous surveys using single point observations provided some statistical evidence for the occurrence of infall within massive cores, blue profiles can also be caused by rotation. Therefore maps of the molecular environment are indispensable. Mapping also allows us to locate the center of the inflow and to identify cores that are simultaneously showing evidence for in- and outflow.

Therefore, we conducted a mapping survey including 46 high mass star-forming regions which were selected applying three criteria: (1) The sources must have been mapped in the submillimeter or millimeter wavelengths with continuum or spectroscopy; (2) signal-to-noise ratios should be  $>5$  at  $350 \mu\text{m}$  (Mueller et al. 2002) and higher at other wavelengths; (3) there should be no other core within one arcmin (Zinchenko, Henning, & Schreyer 1997; Hunter et al. 1998; Tieftrunk et al. 1998; Hatchell et al. 2000; Molinari et al. 2000; Beuther et al. 2002; Mueller et al. 2002). With respect to their stellar content, we can divide the sample into two different groups of targets: (1) Thirty three sources lack 6 cm continuum emission and are precursors of UC HII regions or HMPOs (Molinari et al. 2000; Beuther et al. 2002). Among these, thirty are hosting a luminous IRAS source. The remaining three are associated with IRAC (the InfraRed Array Camera on the Spitzer Space Telescope) point sources (W3-W and W3-SE) or are not hosting an IRAC source (18454–3). All 33 cores comprise

‘group I’. (2) Thirteen UC HII regions are assigned to ‘group II’. This letter presents a list of the identified collapse candidates and provides the statistics of blue excesses. Detailed properties of individual cores will be analyzed in a future paper.

## 2. Observations

The observations were performed with the IRAM 30 m telescope at Pico Veleta, Spain, from July 28 to Aug. 1, 2005. Four receivers were used simultaneously, usually two at  $\lambda \sim 3$  mm and two at  $\lambda \sim 1.3$  mm (A/B configuration). For some sources, none of the four 3 and 1.3 mm lines were optically thin. In these cases the tracer lines were changed employing two receivers at  $\lambda \sim 2$  mm and the other two to cover the upper part of the 1.3 mm window (C/D configuration). The lines and corresponding beam sizes, efficiencies, and channel widths are given in Table 1. The channel spacing and the bandwidth are 78.125 kHz and 105 MHz respectively. The weather was extremely good for summer conditions, allowing us to observe the  $\text{HCO}^+$   $J=3-2$  transition at 268 GHz and leading to 3 and 1.3 mm (2 and 1.2 mm) system temperatures of order 150 and 400 K (200 and 550 K) on a  $T_A^*$  scale. Pointing and calibration were checked by continuum measurements of the standard sources W3(OH), G34.24, and NGC 7027 and were found to be better than  $4''$  and  $\pm 20\%$ , respectively. All observations were carried out in a position switching mode. For each source we observed a nine point map in a cross pattern with a spacing of  $15''$ . If inflow signature was detected, the map was enlarged in most cases to cover the entire region showing this signature. The on-source integration time per position was 1 minute, yielding a  $T_A^* 1\sigma$  noise level of 0.07 K for the 3 mm  $\text{N}_2\text{H}^+$  (1–0) line. For the data analysis, the GILDAS software package (CLASS/GREG) was used (Guilloteau & Lucas 2000).

## 3. Results and discussion

### 3.1. Blue profile identification

For self-absorbed optically thick lines, the classical signature of inflow is a double peaked profile with the blue-shifted peak being stronger, or a line asymmetry with the peak skewed to the blue side. While optically thin lines should show a single velocity component peaking at the line center.

Among the 46 cores observed, five (05490+2658, G31.41+0.31, 18454-3, 18454-4, 19266+1745) will be ignored because they show either too complex spectral profiles, inhibiting a detailed analysis, or a lack of optically thin lines. Estimates of optical depths were obtained from

line ratios between different isotopomers of CO and CS and from the relative intensities of individual hyperfine components in the case of C<sup>17</sup>O and N<sub>2</sub>H<sup>+</sup>. C<sup>18</sup>O, C<sup>17</sup>O, C<sup>34</sup>S and N<sub>2</sub>H<sup>+</sup> tend to be optically thin, while CS is optically thick. HCO<sup>+</sup> opacities could not be estimated. However, the similarity of HCO<sup>+</sup> and CS line shapes (see Sect. 3.2) as well as the results of Gregersen et al. (2000) and FWS05 clearly indicate that HCO<sup>+</sup> is also optically thick.

The 41 remaining sources were detected in at least one optically thick and one optically thin line. A blue profile caused by inflow motion with velocity  $v \propto r^{-1/2}$  in a region with higher excitation temperature ( $T_{ex}$ ) inside requires  $T_A^*(B)/T_A^*(R) > 1$ . Here  $r$  is the radius of the collapsing core (Zhou et al. 1993).  $T_A^*(B)$  and  $T_A^*(R)$  are the blue and red peak intensities of the optically thick line. We also define a dimensionless asymmetry parameter following Mardones et al. (1997),  $\delta V = (V_{thick} - V_{thin})/\Delta V_{thin}$ .  $V_{thick}$  is the peak velocity of the opaque line,  $V_{thin}$  and  $\Delta V_{thin}$  denote the peak velocity and width of the optically thin line. Only for  $\delta V < -0.25$  or  $> 0.25$  the line profile is rated blue or red, respectively.

Our sources (Table 2) discriminate among five main types of line shapes: (1) cores with lines showing a “blue profile” (in the following denoted with B); (2) cores with lines showing a “red profile” (R); (3) cores exhibiting blue and red profiles at different spatial positions (BRS); (4) cores where some lines show a blue profile, while others display a red profile (BRL); (5) cores without obvious asymmetric lines (S). Only cores showing at least one line of type B, but no lines of type R are identified as targets potentially undergoing inflow motion.

### 3.2. Collapse candidates and their profile “excess”

With the criteria outlined in Sect. 3.1, seventeen inflow candidates are identified (see Table 2). Ten belong to group I and seven are part of group II. To provide a typical example, Fig. 1 shows the infall signature of the group I core W3-SE. Fig. 1a displays the HCO<sup>+</sup> (1–0) spectra, showing the angular size of the core. Fig. 1b shows a number of profiles towards the central position. The HCO<sup>+</sup> (1–0) and (3–2) lines as well as the CS (3–2) transition show the blue asymmetry. For the HCO<sup>+</sup> (1–0) line this is also demonstrated in the position-velocity (P-V) diagram of Fig. 1c. For comparison, Fig. 1d shows a P-V diagram of the optically thin C<sup>18</sup>O (1–0) emission.

The quantity “excess” as defined by Mardones et al. (1997) is  $E = (N_B - N_R)/N_T$ , where  $N_B$  and  $N_R$  mark the numbers of sources with blue and red profiles.  $N_T$  is the total number of sources. For our survey the excess was calculated for the two HCO<sup>+</sup> transitions and the

CS (3–2) line. Fig. 2 shows the  $\log[T_A^*(B)/T_A^*(R)]$  and  $\delta V$  (see Sect. 3.1) distributions of the three individual lines. Statistical results are given in Table 3. The observed excess derived from the  $\text{HCO}^+$  (1–0) and (3–2) lines is 0.29 and 0.11, respectively. Both are larger than those obtained by FWS05 for the same lines (0.15 and 0.04). For the CS transition we obtain 0.29. To evaluate the statistical significance of the determined values, we conducted the binomial test (see FWS05 and references therein). Probabilities that the excesses are a product of a random distribution are given in the last column of Table 3. These are 0.006 and 0.01 for  $\text{HCO}^+$  (1–0) and CS (3–2) respectively. Apparently, both lines are sensitive tracers of potential inflow motion in massive cores.

To evaluate differences between the two classes of cores (I and II; see Sect. 1) with respect to the excess, we used the  $\text{HCO}^+$  (1–0) line, which was mapped in the largest number of sources. The results listed in the lower part of Table 3 include 16 sources with profiles of type B. The excesses observed for group I and II are 0.17 and 0.58, respectively.

Twenty of our 46 sources overlap with those of FWS05. Among them are 19 group I sources (out of 33), but only one source is from group II (out of 13). Our study includes various CO and CS lines. We also made maps. Thus we can view the common objects from a different perspective and can check, how far the choice of different molecular transitions and the presence of maps is leading to contradictions with previously published results. Differences are indeed significant. For eight of the 19 overlapping type I cores we obtain different line asymmetry classification, emphasizing the need for detailed maps. Nevertheless, the overall difference in the  $\text{HCO}^+$  (1–0) excess is negligible (0.17 versus 0.15).

To summarize, both data sets indicate that the  $\text{HCO}^+$  (1–0) excess is low for UC HII precursors. For UC HII regions, our results and those of Wyrowski et al. (2006) suggest that the excess is larger and more significant. From the binomial test for group I and II, the probability that the blue excesses (0.17 and 0.58 respectively) are arising by chance is 0.13 and 0.008, respectively.

### 3.3. A comparison with low mass star-forming surveys

While low mass star-forming regions show infall from the Class –I to the Class I stages of evolution, high mass star-forming regions also exhibit infall signatures from their earliest stages till a UC HII region has formed (Wu et al. 2005; Birkmann, Krause, & Lemke 2006; Qin et al. 2006). In low mass cores the profile excess was found to be 0.30, 0.31 and 0.31 for Class –I, 0 and I core samples in the  $\text{HCO}^+$  (3–2) line (Evans (2003) and references therein). There seem to be no significant differences among the cores in different evolutionary phases.

However, our samples show the excess of UC HII regions far surpassing that of the UC HII precursors. This may point to fundamental differences between low and high mass star-forming conditions. Possible causes to the higher blue excess in Group II sources may be: (1) The molecular gas surrounding UC HII regions may be more adequately thermalized to show the blue excess, i.e. the excitation temperature of specific lines may increase more monotonically towards the center. Thus all lines may produce blue profiles indicating infall motion, while in younger cores still some lines may show red profiles. (2) The amount of dense cool gas is larger towards younger objects. Outflows of dense molecular gas may be more active around Group I objects, shaping more red profiles. (3) Low mass cores are relatively isolated and their gas supply is limited. Simulations showed that this may halt the increase of inflow (Vorobyov 2005). However, high mass stars form in giant molecular clouds and their inflow motions are not easily halted by the exhaustion of molecular gas before most of it is dispelled. (4) In low mass cores, star formation may be spontaneous. In high mass cores, collapse may be triggered by extrinsic disturbances and the collapse may take more time to develop.

With respect to potential selection effects, we used the same criteria to identify the targets of the two separate groups of sources. Since this study is based on a limited number of sources, more data quantifying the blue excess as a function of evolutionary stage would be highly desirable.

#### 4. Outlook

We have carried out a mapping survey towards 46 molecular cores associated with massive star formation. Seventeen collapse candidates were identified. Among them are 10 UC HII precursors and 7 UC HII regions. Overall, statistical results indicate a predominance of blue over red profiles which is surprisingly similar to that obtained towards cores forming low mass stars. Among high mass star-forming sites, the probability to detect blue profiles seems to depend on evolutionary stage and increases from UC HII precursors to UC HII regions. Toward low mass star-forming sites, however, this effect is not observed, suggesting a more fundamental difference in the way stellar masses are assembled. Larger line surveys and more detailed maps in various molecular transitions are needed to improve statistical evidence in order to confirm or to reject this potentially important finding.

We are grateful to the IRAM staff for their assistance and F. Wyrowski for useful discussions. This research is supported by the Grant 10128306 and 10733030 of NSFC.

## REFERENCES

- Beuther, H., Schilke, P., Menten, K. M., Motte, F., Sridharan, T. K., & Wyrowski, F. 2002, *ApJ*, 566, 945
- Birkmann, S. M., Krause, O., & Lemke, D. 2006, *ApJ*, 637, 380
- Brand, J., & Blitz, L. 1993, *ApJ*, 275, 67
- Evans, N. J. II, in *Chemistry as a Diagnostic of Star Formation*, eds. C. L. Curry & M. Fich, NRC Press, Ottawa, Canada, 2003, p. 157
- Fuller, G. A., Williams, S. J., & Sridharan, T. K. 2005, *A&A*, 442, 949 (FWS05)
- Gregersen, E. M., Evans, N. J. II, Mardones, D., & Myers, P. C. 2000, *ApJ*, 533, 440
- Guilloteau, S. & Lucas, R. 2000, in *Imaging at Radio through Submillimeter Wavelengths*, eds. J.G. Mangum & S. Radford, ASP Conf. Ser., 217, 299
- Hatchell, J., Fuller, G. A., Millar, T. J., Thompson, M. A., & Macdonald, G. H. 2000, *A&A*, 357, 637
- Hughes, V. A. & MacLeod, G. C. 1994, *ApJ*, 427, 857
- Hunter, T. R., Neugebauer, G., Benford, D. J., Matthews, K., Lis, D. C., Serabyn, E., & Phillips, T. G. 1998, *ApJ*, 493, L97
- Lee, C. Myers, P. C., & Tafalla, M. 1999, *ApJ*, 526, 788
- Lockman, F. J. 1989, *ApJS*, 71, 469
- Mardones, D., Myers, P. C., Tafalla, M., Wilner, D. J., Bachiller, R., & Garay, G. 1997, *ApJ*, 489, 719
- Molinari, S., Brand, J., Cesaroni, R., & Palla, F. 2000, *A&A*, 355, 617
- Mueller, K. E., Shirley, Y. L., Evans, N. J., II, & Jacobson, H. R. 2002, *ApJS*, 143, 469
- Qin et al. 2006, in *Journal of Phys. Conf. Ser. 54, Galaxy Center Workshop*, IOP pub., P. 468
- Sridharan, T. K., Beuther, H., Schilke, P., Menten, K. M., & Wyrowski, F. 2002, *ApJ*, 566, 931
- Tieftrunk, A. R., Megeath, S. T., Wilson, T. L., & Rayner, J. T. 1998, *A&A*, 336, 991

- Vorobyov, E. I. & Basu, S. 2005, MNRAS, 363, 1361
- Wolfire, M. G., & Cassinelli, J. P. 1987, ApJ, 319, 850
- Wu, J., & Evans, N. J., II 2003, ApJ, 592, L79
- Wu, Y., Zhu, M., Xu, D., Wei, Y., & Zhu, L., 2005, in IAUS 227, Eds: R. Cesaroni, M. Felli, E. Churchwell & M. Walmsley, Cambridge U. Press, Acireale, Italy, P. 225
- Wu, Y., Zhang, Q., Yu, W., Miller, M., Mao, R., Sun, K., & Wang, Y. 2006, A&A, 450, 607
- Wyrowski, F., Heyminck, S., Güsten, R., & Menten, K. M. 2006, A&A, 454, L95
- Zhou, S., Evans, N. J. II, Koempe, C., & Walmsley, C. M. 1993, ApJ, 404, 232
- Zinchenko, I., Henning, T., & Schreyer, K. 1997, A&AS, 124, 385



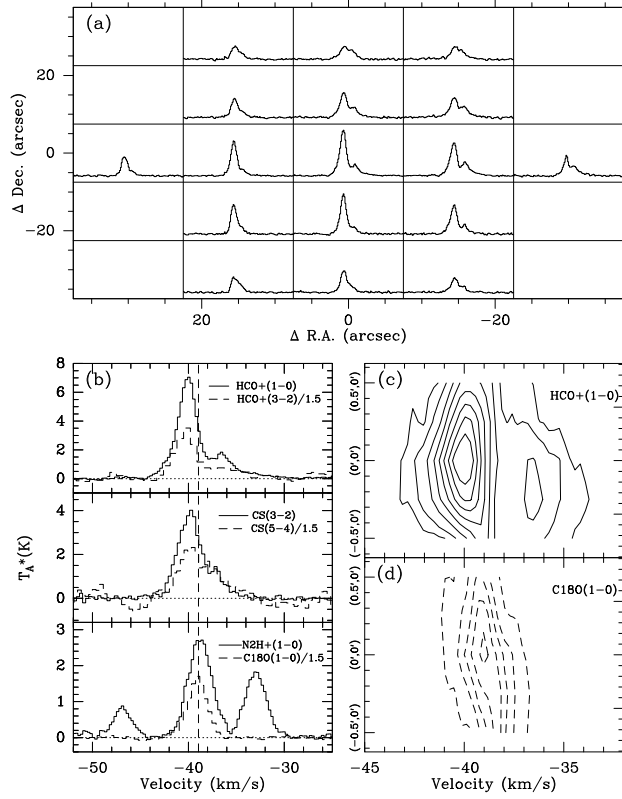


Fig. 1.— W3-SE. **a.**  $\text{HCO}^+$  (1–0) grid. The X and Y axes denote R.A. and Dec. offsets in arcseconds relative to the  $\text{NH}_3$  peak position of Tieftunk et al. (1998). **b.** Spectra towards the central position. Molecular species and transition are given at the upper-right corner of each inset. **c.** Position-velocity diagram of the optically thick  $\text{HCO}^+$  (1–0) line along  $\Delta\text{Dec.} = 0$ . Contour levels are 0.5 K ( $3\sigma$ ) and 1.0 to 5.8 K by 0.8 K. **d.** Position-velocity diagram of the optically thin  $\text{C}^{18}\text{O}$  (1–0) line along  $\Delta\text{Dec.} = 0$ . Contour levels are 0.3 K ( $3\sigma$ ) and 1.0 to 2.5 K by 0.5 K.

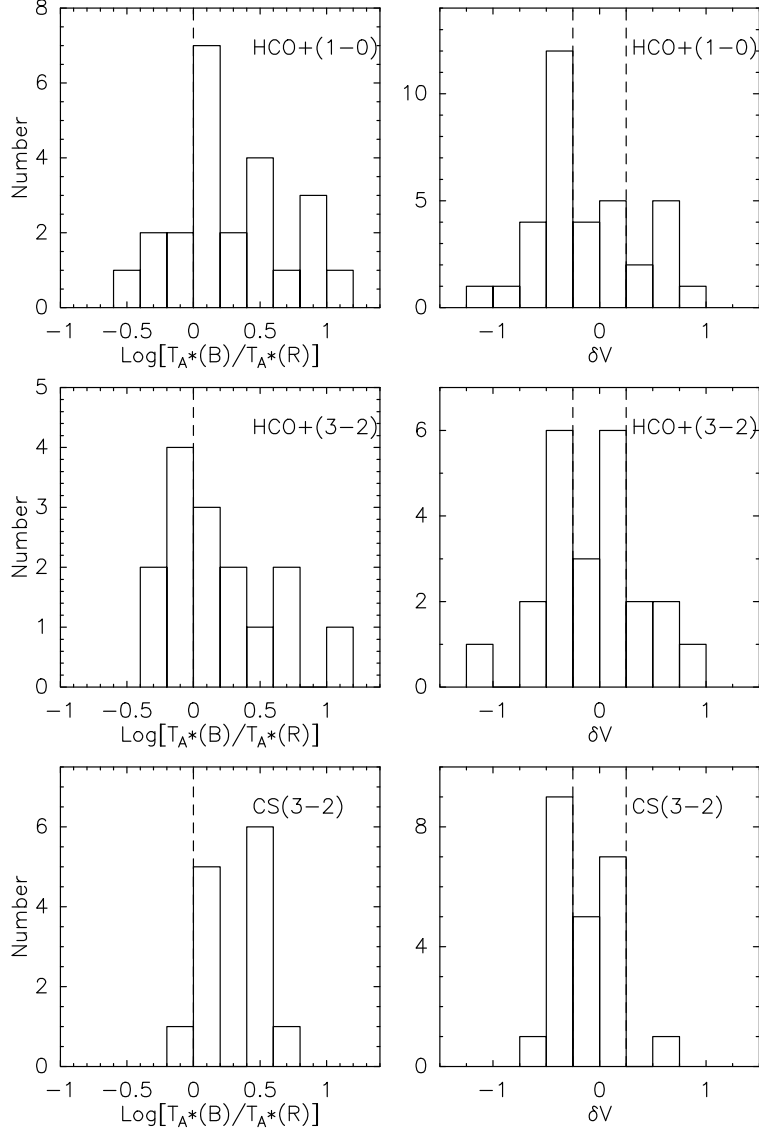


Fig. 2.— The distribution of  $\log [T_A^*(B)/T_A^*(R)]$  (left; ratio of blue versus red peak intensity) and  $\delta V$  (right; the line asymmetry parameter, see Sect. 3.1). The upper, middle and lower panels show results from  $\text{HCO}^+(1-0)$ ,  $\text{HCO}^+(3-2)$  and  $\text{CS}(3-2)$ , respectively. There is a total of 41 cores observed in the  $\text{HCO}^+(1-0)$ , 28 in the  $\text{HCO}^+(3-2)$ , and 28 in the  $\text{CS}(3-2)$  line. For the  $\delta V$  histograms, BRS sources (for a definition, see Sect. 3.1) had to be excluded (6, 5, and 5 in the three transitions, respectively). There are additional 12, 8, and 10 cores, for which no blue versus red peak intensity ratio could be obtained.

Table 1. Observed lines<sup>a)</sup>

No.	Line	Frequency (GHz)	HPBW (arcsec)	$\eta_{\text{mb}}$	$\Delta V_{\text{res}}$ (km s <sup>-1</sup> )
1	$\text{HCO}^+(1-0)$	89.18852	27.6	0.77	0.263
2	$\text{HCO}^+(3-2)$	267.55763	9.2	0.45	0.112
3	$\text{CS}(3-2)$	146.96905	16.7	0.69	0.159
4	$\text{CS}(5-4)$	244.93561	10.0	0.49	0.122
5	$\text{N}_2\text{H}^+(1-0)$	93.17378	26.4	0.77	0.251
6	$\text{C}^{18}\text{O}(1-0)$	109.78218	22.4	0.75	0.213
7	$\text{C}^{18}\text{O}(2-1)$	219.56033	11.2	0.55	0.137
8	$\text{C}^{17}\text{O}(1-0)$	112.35928	21.9	0.74	0.209
9	$\text{C}^{17}\text{O}(2-1)$	224.71437	10.9	0.54	0.133
10	$\text{C}^{34}\text{S}(5-4)$	241.01618	10.2	0.50	0.122

a) HPBW: half power beamwidth;  $\eta_{\text{mb}}$ : beam efficiency;  
 $\Delta V_{\text{res}}$ : channel width

Table 2. Profiles of the observed sources

Source Name <sup>a</sup>	$\alpha^b$ J2000	$\delta^b$ J2000	$D^c$ (kpc)	Profile <sup>d</sup>	Ref.	Source Name <sup>a</sup>	$\alpha^b$ J2000	$\delta^b$ J2000	$D^c$ (kpc)	Profile <sup>d</sup>	Ref.
W3-W <sup>I</sup>	02 25 32.4	+62 06 01	1.95	<i>B</i>	1	18488+0000SE <sup>I</sup>	18 51 25.6	+00 04 07	5.4	<i>BRL</i>	3,7
W3-C <sup>II</sup>	02 25 39.5	+62 05 51	2.3	<i>BRS</i>	1	G34.26+0.15 <sup>II</sup>	18 53 18.4	+01 14 56	3.7	<i>In, B</i>	6
W3-SE <sup>I</sup>	02 25 54.5	+62 04 11	2.3	<i>B</i>	1	18521+0134 <sup>I</sup>	18 54 40.8	+01 38 02	5.0	<i>B</i>	3,7
05358+3543 <sup>I</sup>	05 39 10.4	+35 45 19	1.8	<i>BRS</i>	3,7	18530+0215 <sup>I</sup>	18 55 34.2	+02 19 08	5.1	<i>S</i>	3,7
05490+2658 <sup>I</sup>	05 52 12.9	+26 59 33	2.1	...	3,7	S76E <sup>II</sup>	18 56 11.0	+07 53 28	2.1	<i>S?</i>	4,9
G10.47+0.03 <sup>II</sup>	18 08 38.2	−19 51 50	5.8	<i>B</i>	10	18553+0414NE <sup>I</sup>	18 57 53.4	+04 18 15	0.6	<i>B</i>	3,7
G12.42+0.50 <sup>II</sup>	18 10 51.8	−17 55 56	2.1	<i>B</i>	2	19012+0536 <sup>I</sup>	19 03 45.1	+05 40 40	4.6	<i>B</i>	3,7
G12.89+0.49 <sup>II</sup>	18 11 51.3	−17 31 29	3.5	<i>BRL</i>	2,3,9	19092+0841SW <sup>I</sup>	19 11 36.7	+08 46 20	4.48	<i>BRL</i>	5
G13.87+0.28 <sup>II</sup>	18 14 35.4	−16 45 37	4.4	<i>S?</i>	10	G43.89-0.79 <sup>II</sup>	19 14 26.2	+09 22 34	4.2	<i>B</i>	10
18144-1723NW <sup>I</sup>	18 17 23.8	−17 22 09	4.33	<i>R</i>	5	19217+1651N <sup>I</sup>	19 23 58.8	+16 57 45	10.5	<i>B</i>	3,7
18182-1433 <sup>I</sup>	18 21 07.9	−14 31 53	4.5	<i>B</i>	3,7	19266+1745 <sup>I</sup>	19 28 54.0	+17 51 56	0.3	...	3,7
G19.61 <sup>I</sup>	18 27 37.9	−11 56 07	4.0	<i>S?</i>	2	19410+2336 <sup>I</sup>	19 43 11.4	+23 44 06	2.1	<i>B</i>	3,7
18264-1152 <sup>I</sup>	18 29 14.3	−11 50 26	3.5	<i>R</i>	3,7	S86SE <sup>I</sup>	19 43 49.7	+23 28 41	1.9	<i>BRS</i>	4
18306-0835 <sup>I</sup>	18 33 21.8	−08 33 38	4.9	<i>R</i>	3,7	S87N <sup>I</sup>	19 46 20.6	+24 36 04	2.3	<i>S?</i>	4
G24.49-0.04 <sup>II</sup>	18 36 05.3	−07 31 23	3.5	<i>B</i>	2,11	20126+4104 <sup>I</sup>	20 14 26.0	+41 13 32	1.7	<i>S?</i>	3,7
18337-0743NE <sup>I</sup>	18 36 40.9	−07 39 20	4.0	<i>BRL</i>	3	20216+4107 <sup>I</sup>	20 23 23.8	+41 17 40	1.7	<i>S</i>	3,7
18355-0650 <sup>II,*</sup>	18 38 14.2	−06 47 47	4.2	<i>B</i>	8	20319+3958 <sup>I</sup>	20 33 49.3	+40 08 45	1.6	<i>S</i>	3,7
18372-0541 <sup>I</sup>	18 39 56.0	−05 38 49	1.8	<i>B</i>	3,7	22134+5834 <sup>I</sup>	22 15 09.1	+58 49 09	2.6	<i>BRS</i>	3,7
18385-0512E <sup>I</sup>	18 41 13.3	−05 09 06	2.0	<i>R</i>	3,7	23033+5951 <sup>I</sup>	23 05 25.7	+60 08 08	3.5	<i>S?</i>	3,7
G31.41+0.31 <sup>II</sup>	18 47 34.7	−01 12 46	7.9	...	10	NGC7538-11 <sup>I</sup>	23 13 44.7	+61 26 54	2.8	<i>B</i>	2
18454-3 <sup>I</sup>	18 47 55.9	−01 53 35	5.6	...	3,7	NGC7538-N <sup>II</sup>	23 13 45.4	+61 28 12	2.8	<i>B</i>	2
18454-4 <sup>I</sup>	18 48 01.4	−01 52 37	5.6	...	3,7	23139+5939 <sup>I</sup>	23 16 09.3	+59 55 23	4.8	<i>BRS</i>	3,7
18470-0044 <sup>I</sup>	18 49 36.7	+00 41 05	8.2	<i>R</i>	3,7	23151+5912 <sup>I</sup>	23 17 21.0	+59 28 49	5.7	<i>BRS?</i>	3,7

<sup>a</sup>Indices “I” and “II”, attached to the source names, denote group I and II, respectively (see Sect. 1). “\*” denotes the optical thin line is quoted from Luo & Wu (2007, in preparation); b. The positions are taken from the references (last column). c. If there is no distance available for a core, the distance is calculated using the galactic rotation curve of Brand & Blitz (1993). If there is a distance ambiguity, the nearer one is chosen. d. Type of detected line profile (Sect. 3.1 for definitions). References: 1. Tieftrunk et al. (1998); 2. Mueller et al. (2002); 3. Beuther et al. (2002) and references therein; 4. Zinchenko et al. (1997); 5. Molinari et al. (2000); 6. Hunter et al. (1998); 7. Sridharan et al. (2002); 8. Wu et al. (2006) and the references therein; 9. Hughes & MacLeod (1994); 10. Hatchell et al. (2000); 11. Lockman 1989.

Table 3. Blue excess statistics

Line/Source	$N_B$	$N_R$	$N_T$	$E$	$p$
Results from selected lines					
HCO <sup>+</sup> (1–0)	16	4	41	0.29	0.006
HCO <sup>+</sup> (3–2)	8	5	28	0.11	0.29
CS (3–2)	9	1	28	0.29	0.01
HCO <sup>+</sup> (1–0) line results w.r.t. source properties					
Group I	9	4	29	0.17	0.13
Group II	7	0	12	0.58	0.008
Total	16	4	41	0.29	0.006

$N_B$ : Number of "blue" profiles;  $N_R$ : Number of "red" profiles;  $N_T$ : Total number of observed sources.  $E$ : Excess;  $p$ : statistical likelihood that the result is caused by random fluctuations (see Sect.3.2). Note that only 15 of the 17 inflow candidates show blue profiles in the HCO<sup>+</sup> (1–0) line. The other two are identified by CS (3–2) and HCO<sup>+</sup> (3–2) spectrum, respectively. One of the 16 HCO<sup>+</sup> (1–0) blue profiles is a "BRL" source (see Sect.3.1).